Optimization Design of High-speed Interior Permanent Magnet Motor with High Torque Performance Based on Multiple Surrogate Models

Shengnan Wu, *Member, IEEE*, Xiangde Sun, and Wenming Tong, *Member*, *IEEE*

***Abstract*—In order to obtain better torque performance of high-speed interior permanent magnet motor(HSIPMM) and solve the problem that electromagnetic optimization design is seriously limited by its mechanical strength, a complete optimization design method is proposed in this paper. The object of optimization design is a 15kW、20000r/min HSIPMM whose permanent magnets in rotor is segmented. Eight structural dimensions are selected as its optimization variables. After design of experiment(DOE), multiple surrogate models are fitted, a set of surrogate models with minimum error is selected by using error evaluation indexes to optimize, the NSGA-II algorithm is used to get the optimal solution. The optimal solution is verified by load test on a 15kW, 20000 r/min HSIPMM prototype. This paper can be used as a reference for the optimization design of HSIPMM.**

***Index Terms*—High-speed interior permanent magnet motor, Segmented magnets, Multi-objective optimization, Multiple surrogate models.**

I. Introduction

HIGH-SPEED permanent magnet motor has the advantages of high power density, high efficiency and can directly drive high speed equipment. It has broad development prospects in the field of new energy vehicles, flywheel energy storage and aerospace[1]-[2]. High-speed permanent magnet motor is divided into surface-mounted and interior-mounted. Compared with surface-mounted, interior-mounted permanent magnet motor has better torque performance, higher power density, better speed regulation performance and lower cost[3]. However, the mechanical performance of the high speed interior permanent magnet motor(HSIPMM) is poor and its poor mechanical performance often makes the electromagnetic optimized results fail to meet the mechanical properties. Therefore, the optimization of the HSIPMM has high engineering value and practical significance.

At present, experts and scholars from various countries have adopted a variety of methods for permanent magnet motor optimization design. In [4], the maximum average torque, minimum torque ripple and minimum cogging torque of the motor are taken as the optimization objectives, and Taguchi method is used to optimize the motor. Finally, the optimized rotor structure parameters are obtained. In [5], the electromagnetic and mechanical properties (calculated by analytical method) of a surface mounted high-speed permanent magnet motor are optimized by using multi-objective genetic algorithm based on ANSYS workbench platform, and the expected target performance is finally achieved. In [6], Taguchi method, genetic algorithm and hybrid genetic algorithm are used to optimize the rotor structure of the interior permanent magnet motor for electric vehicles, so as to optimize the performance of the motor such as torque, torque ripple, iron loss and efficiency. Some of the optimization methods in the above literature have insufficient optimization accuracy, and some require a large number of finite element calculation, while the HSIPMM requires a lot of time for each electromagnetic and mechanical stress simulation, so the above optimization methods are not applicable to the HSIPMM.

In order to save the simulation time, the efficiency of a vehicle amorphous alloy permanent magnet motor is optimized by fitting the response surface surrogate model in [7], which save a lot of simulation time, but the fitting error is not mentioned. In [8], a low-speed interior permanent magnet motor is optimized, three different surrogate models are fitted and the fitting errors of three different surrogate models are compared, the optimal surrogate model is selected to ensure the feasibility of optimization. However, this method does not consider the mechanical stress problem, so it is not suitable for the HSIPMM, and the above literature did not consider the structural change in the optimization process will lead to the maximum torque appear at different internal power factor angles.

In order to solve the problem that the electromagnetic optimization of the HSIPMM is limited by the mechanical strength, this paper takes the optimization design of a 15 kW, 20000 r/min high-speed motorized spindle drive motor for

Manuscript received July Manuscript received, 2022; revised August 02, 2022; accepted August 15, 2022. date of publication September 25, 2022; date of current version September 18, 2022.

This work has been supported by the National Natural Science Foundation of China (51907129); Project Supported by Department of Science and Technology of Liaoning Province (2021-MS-236).*(Corresponding Author: Shengnan Wu)*

Shengnan Wu is with the School of Electrical Engineering, Shenyang University of Technology, Shenyang 110870, China (e-mail: imwushengnan@163.com).

Xiangde Sun is with the School of Electrical Engineering, Shenyang University of Technology, Shenyang 110870, China (e-mail: xiangde.s@foxmail.com).

Wenming Tong is with the National Engineering Research Center for Rare Earth Permanent Magnet Machines, Shenyang University of Technology, Shenyang 110870, China (e-mail: twm822@126.com).

Digital Object Identifier 10.30941/CESTEMS.2022.00033

machine tools as an example, and a complete optimization design method of the HSIPMM is proposed.

Firstly, the initial scheme of the motor is designed, and eight structural dimensions of the motor are selected as variables. Then the electromagnetic data and mechanical stress of the motor are calculated by finite element method after design of experiment(DOE). The obtained data are fitted by surrogate models, and the multi-objective optimization is carried out with high efficiency and low cost as the objective function.

II. Initial Design of Motor

TABLE I
INITIAL SCHEME OF MOTOR DESIGN

Items	Values
Rated power P(kW)	15
Rated voltage U(V)	380
Rated speed n(r/min)	20000
Stator outer radius r_1(mm)	70
Stator inter radius r_a(mm)	35
Core length L(mm)	110
Air-gap length δ(mm)	1
PM width B_m(mm)	13.5
PM thickness H_m(mm)	4.5
Reinforcing bar width j(mm)	1.6
Magnetic bridge width b(mm)	1.4
Half of the distance between PM slots c(mm)	3
Number of stator slots Z	18
Slot height h(mm)	11.5
Number of poles $2p$	4
Efficiency η(%)	96.34
Output torque T_{out}(N·m)	7.19

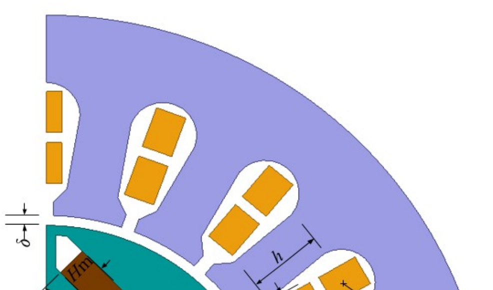

Fig. 1. 1/4 model of motor.

Considering the power, speed and application background of the motor, the materials and basic structure of the motor are determined. Stator core adopts amorphous alloy material to reduce iron loss. The stator slot type adopts pear-shaped slot, and stator teeth are parallel teeth. The permanent magnet adopts NdFeB. In order to have better mechanical properties, the rotor permanent magnet adopts segmented structure. The iron core between the permanent magnet after segmentation is called the reinforcing bar. The appearance of the reinforcing bars increase the leakage of the rotor, which is not conducive to the electromagnetic performance[9]. Therefore, the reinforcing bars should not be too wide. Table I is the initial scheme for motor design. Fig.1 shows the 1/4 model of the motor, and the size of the variables is marked on the model.

III. Multi-objective Optimization Design of Motor

A. Selection of optimization variables and range

It is very important to select the appropriate variables in the process of motor optimization. Too many variables will lead to a large increase in the amount of calculation, while too few variables will limit the optimization results. The optimization of this paper is based on the premise that the main structure of the motor is unchanged, that is, the number of poles and slots is unchanged, and the main size of the motor is unchanged.

In this paper, eight structural dimensions of the motor are selected as optimization variables: air gap length δ is an important factor affecting the optimization results, such as torque and loss; permanent magnet width B_m and permanent magnet thickness H_m are key factors determining the main magnetic field intensity; reinforcing bar width j and magnetic bridge width b are key factors affecting the rotor mechanical strength and magnetic flux leakage; half of the distance between permanent magnet slots c is also an important factor affecting torque; stator outer radius r_1, slot height h and slot width b_{11} are key factors determining the magnetic density of stator teeth and yoke. But the stator slot width b_{11} is determined by slot height h, so it is not taken as a variable. Their relationship can be expressed as:

$$b_{11}=\frac{2}{h}\left(A_s-\frac{\pi r_s^2}{2}\right)-2r_s \tag{1}$$

where r_s is the bottom radius of the slot, A_s is the slot area, and the slot area remains constant in the optimization process.

The range of optimization variables is shown in Table II:

TABLE II
THE RANGE OF OPTIMIZATION VARIABLES

Items	Values
Air-gap length δ(mm)	[1,2]
PM thickness H_m(mm)	[4,6]
PM width B_m(mm)	[13,16]
Reinforcing bar width j	[1,2]
Magnetic bridge width b(mm)	[0.8,1.6]
Half of the distance between PM slots c(mm)	[2.5,4]
Slot height h(mm)	[10.5,12]
Stator outer radius r_1(mm)	[60,70]

B. Optimization objectives and constraints

The evaluation of motor quality needs to be considered from two aspects: performance index and economic index. The performance index of this paper selects the efficiency of motor, and the economic index selects the effective cost of motor. So the optimization objectives are the maximum efficiency of motor under rated operating conditions and the lowest effective cost.

$$\begin{cases}\max(\eta)\\ \min(Cost)\end{cases} \tag{2}$$

The efficiency η can be calculated as:

$$\eta = \frac{P_{out}}{P_{out} + p_{Fe} + p_{Cu} + p_{fw} + p_{ad}} \tag{3}$$

where P_{out}, p_{Fe}, p_{cu}, p_{fw} and p_{ad} are output power, stator iron loss, copper loss, mechanical loss and additional loss, respectively. The mechanical loss is the sum of wind friction loss and bearing loss, which is calculated by analytical formula, and the others are calculated by finite element method.

The wind friction loss can be expressed as[10]:

$$p_w = \pi C_d \rho_f \omega^3 r^4 L \tag{4}$$

where C_d is the friction coefficient of rotor surface, ρ_f is the fluid density; ω is angular velocity; r is the rotor radius.

The bearing loss can be expressed as[11]:

$$p_b = C_b D_b^3 \omega \tag{5}$$

where C_b is the friction coefficient of the bearing, provided by the manufacturer, D_b is the diameter of the bearing.

The effective cost can be given by

$$Cost = C_{Fe} W_{Fe} + C_{PM} W_{PM} + C_{Cu} W_{Cu} \tag{6}$$

where C_{Fe}, C_{PM} and C_{Cu} are the price per kg of amorphous alloy core, permanent magnet and copper winding, respectively; W_{Fe}, W_{PM} and W_{Cu} are the mass of stator amorphous alloy, permanent magnet and copper winding, respectively.

After the optimization objectives are determined, it is necessary to determine the constraints of motor optimization. The most important constraint is the maximum mechanical stress of the rotor. ANSYS Workbench software is used to calculate the rotor stress. Considering the weak magnetic speed regulation, when calculating the stress, the speed is 24000r/min. In order to improve the calculation speed, the model adopts a half model, and displacement constraints are used on the segmented surface to limit the tangential displacement. Secondly, it is necessary to ensure sufficient output torque. Table III lists the optimization constrains.

TABLE III
RESTRAINT CONDITIONS OF MOTOR

Items	Values
Output torque	$T_{out} \geq 7.16$N·m
Maximum equivalent stress of rotor core	$\sigma_{max} \leq 343$MPa

C. Optimization process

The optimization flow chart of the motor is shown in Fig. 2.

DOE is the first step to optimize using surrogate models. The theoretical basis of DOE is probability theory and mathematical statistics. To construct a surrogate model with small error, it is necessary to ensure that the sampling points are distributed in all the design space. The DOE method used in this paper is Central Composite Design(CCD). With the help of Response Surface module in ANSYS workbench, this module contains some common DOE methods, which can automatically generate design table and generate 81 sample points.

Fig.3 is the calculation flow chart of each sample point in workbench. In the figure, Psi is the internal power factor angle. Due to the structural change of the motor in the optimization process, the maximum torque will occur at different internal power factor angles. After the calculation of the whole process, it will be compared in the Parameter Set module, and the internal power factor angle of the maximum torque will be selected. The electromagnetic data calculated by this internal power factor angle is used as the electromagnetic data of the sample point. It can be seen from Fig.3 that each sample point requires a lot of finite element calculation and takes a lot of time, so it is better to use surrogate models to optimize.

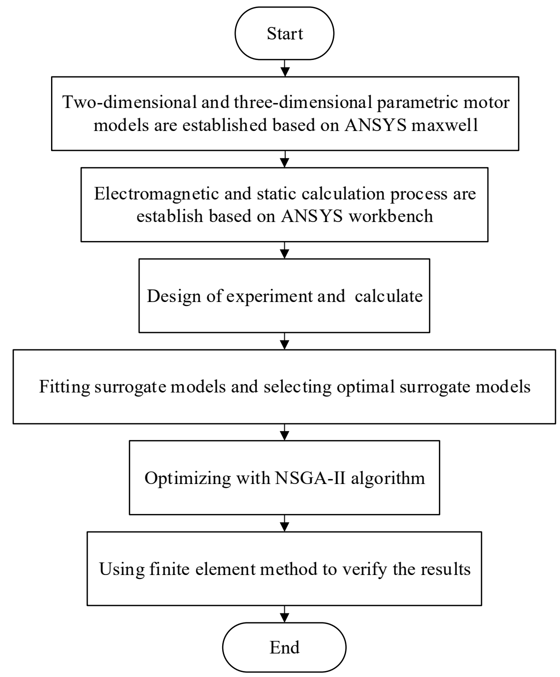

Fig. 2. Electromagnetic and mechanical optimization flow chart of motor

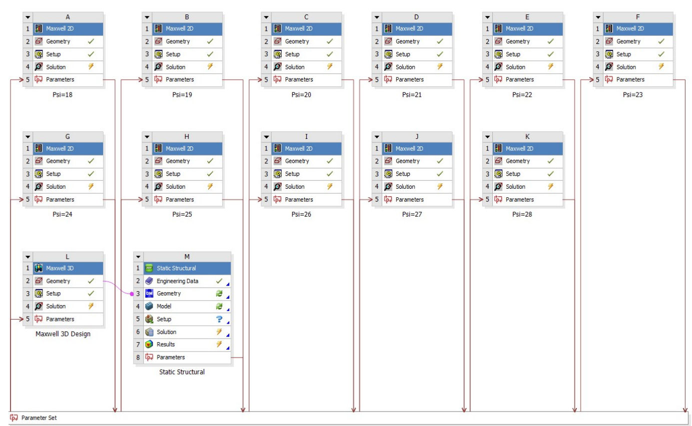

Fig. 3. Calculation flow chart of each sample point

When the data of all sample points are fitted into the surrogate models, the prediction accuracy of the surrogate models are crucial, which is related to the rationality and feasibility of the optimization. In this paper, four common surrogate models are selected for choosing the best, which are first-order response surface model, second-order response surface model, Kriging model and RBF neural network model. Then calculating the fitting errors of four surrogate models for each fitting target, and selecting the surrogate models with the smallest fitting error.

The error evaluation indexes used in this paper are Mean Absolute Error(MAE), Mean Absolute Percentage Error(MAPE), Mean Square Error(MSE) and Coefficient of Determination(R^2).

In order to calculate the fitting errors of each surrogate model, additional 20 sample points are selected for error calculation. Table IV-VII are the fitting errors of different surrogate models:

TABLE IV
FITTING ERRORS OF FIRST-ORDER RESPONSE SURFACE MODEL

	R^2	MAE	MAPE	MSE
Maximum equivalent stress of rotor core	0.8392	22.5432	6.06%	825.1049
Stator iron loss	0.9091	7.7873	3.46%	79.1800
Rotor eddy current loss	0.8640	0.5770	15.80%	0.4983
Output torque	0.9873	0.0731	0.57%	0.0080

TABLE V
FITTING ERRORS OF SECOND-ORDER RESPONSE SURFACE MODEL

	R^2	MAE	MAPE	MSE
Maximum equivalent stress of rotor core	0.8707	20.0283	5.40%	663.3503
Stator iron loss	0	28.1891	11.90%	1156.5790
Rotor eddy current loss	0.9617	0.3025	7.66%	0.1402
Output torque	0.9995	0.0136	0.11%	0.0003

TABLE VI
FITTING ERRORS OF KRIGING MODEL

	R^2	MAE	MAPE	MSE
Maximum equivalent stress of rotor core	0.8056	24.2961	6.32%	997.50
Stator iron loss	0.7925	11.6482	5.05%	180.8076
Rotor eddy current loss	0.9570	0.3338	7.97%	0.1575
Output torque	0.9540	0.1280	0.99%	0.0291

TABLE VII
FITTING ERRORS OF RBF NEURAL NETWORK MODEL

	R^2	MAE	MAPE	MSE
Maximum equivalent stress of rotor core	0.9352	13.8593	3.71%	332.6418
Stator iron loss	0.7327	11.7862	4.99%	232.8749
Rotor eddy current loss	0.9919	0.1550	3.41%	0.0296
Output torque	0.9982	0.0305	0.23%	0.0011

After comparison, the maximum equivalent stress of rotor core and rotor eddy current loss adopt the RBF neural network model, the output torque adopts the second-order response surface model, and the stator iron loss adopts the first-order response surface model.

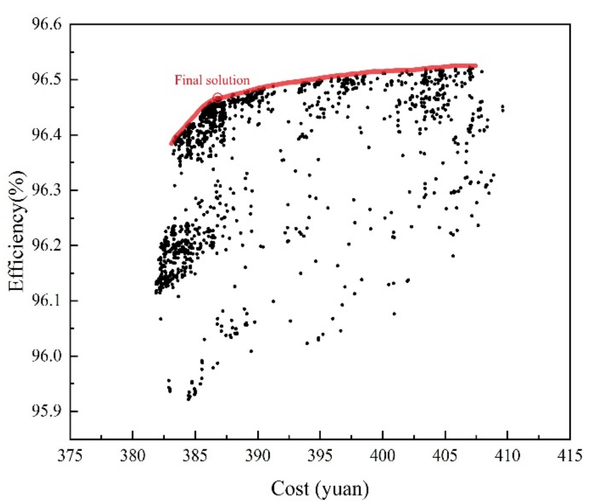

Fig. 4. Optimization results of High-Speed Interior Permanent Magnet Motor

After fitting the surrogate models, NSGA-II multi-objective genetic algorithm is used for global optimization. It supports multiple objectives and constrains, and aims to find the global optimization, so it is very suitable for this paper. The population size of NSGA- II algorithm in this paper is 40, the maximum number of iterations is 50, the crossover probability is 0.9, and the mutation probability is 0.02. The optimized result of NSGA-II multi-objective genetic algorithm is shown in Fig. 4. The red line is the optimal solutions that can be achieved under the constraint conditions, which is called Pareto front. It can be seen from the figure that efficiency and cost are contradictory, and efficiency increases nonlinearly with the increase of cost, which is similar to the B-H curve of iron core. Therefore, it is most favorable to take the position of the knee point of the curve as the final solution, that is, the point in the circle is the final result of optimization.

D. Comparison between optimization results and initial design

Table VIII is the comparison table between the optimization result and the initial design. The optimized values in the table are calculated by using the surrogate models， but the values in brackets are obtained by finite element calculation. It can be seen that the values calculated by finite element method are very close to the predicted value by the surrogate models. After optimization, the efficiency and effective cost of the motor are improved, the efficiency increased from 96.34% to 96.47%, increased by 0.13%, and the effective cost decreased from 402.33 yuan to 386.89 yuan, decreased by 3.84%.

TABLE VIII
COMPARISON TABLE BETWEEN OPTIMIZATION RESULTS AND INITIAL DESIGN

Items	Initial	Optimal
Air-gap length δ(mm)	1	1.3
PM width B_m(mm)	13.5	15
PM thickness H_m(mm)	4.5	4
Reinforcing bar width j(mm)	1.6	1.3
Magnetic bridge width b(mm)	1.4	1.4
Half of the distance between PM slots c(mm)	3	3.7
Slot height h(mm)	11.5	10.7
Stator outer radius r_1(mm)	70	65
Efficiency η(%)	96.34	96.46(96.47)
Cost(yuan)	402.33	386.89
Maximum equivalent stress of rotor core σ_{max} (MPa)	304.01	338.01(332.70)
Output torque T_{out}(N·m)	7.19	7.24(7.24)

Fig. 5 shows the comparison of the output torque before and after optimization. It can be seen that not only the optimized output torque increased by 0.05Nm on average, but also the torque ripple decreased from 7.34% to 4.82%, decreased by 2.52%.

Fig. 6 is the equivalent stress distribution map of the optimized motor rotor. The maximum equivalent stress occurs at the top of the reinforcing bar, which is 332.7MPa.

IV. EXPERIMENTAL TESTS

Based on the above optimization analysis, the prototype is manufactured. In order to measure the efficiency of the prototype, the load experiment of the motor is carried out. The back-to-back experimental method is adopted as shown in Fig.7.

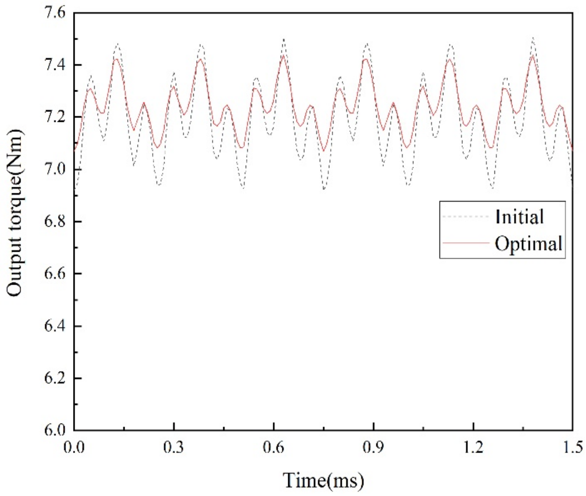

Fig. 5. Comparison of output torque before and after optimization.

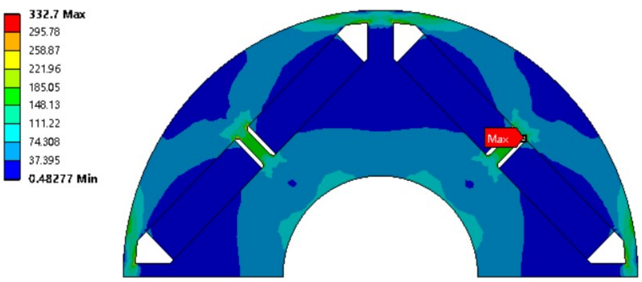

Fig. 6. Equivalent stress distribution of rotor.

Fig. 7. Back to back test bench of high speed permanent magnet motor.

There are two identical motors, one as motor and the other as generator. During the experiment, the speed of motor is constant, the resistance box is used as the load of the generator, and the output power can be adjusted by changing the resistance value of the resistance box. The input power of the motor minus the output power of the generator is the sum of the losses of the two motors. Since the losses of the two motors are the same, the efficiency of the motor can be easily obtained.

Based on the back to back test bench, the efficiency of the motor at the rated speed of 20000r/min was tested, as shown in table IX. It can be seen from the table IX that the experimental values are very close to the calculated values, so the optimization method in this paper is feasible.

TABLE IX
RATED WORKING PERFORMANCE OF ROTOTYPE

P_1(kW)	P_2(kW)	Measured η(%)	Calculated η(%)
16.98	16.35	96.26	96.24
15.54	14.99	96.49	96.47
14.61	14.09	96.41	96.40
13.02	12.52	96.16	96.16
11.31	10.89	96.24	96.19
10.41	10.02	96.21	96.18
8.49	8.13	95.70	95.68
6.2	5.87	94.68	94.65
3.6	3.29	91.53	91.50
1.86	1.33	85.75	85.71

V. CONCLUSION

In this paper, a 15kW, 20000r/min high-speed interior permanent magnet motor was taken as an example, a complete optimization design method for high-speed interior permanent magnet motor is proposed. Firstly, the electromagnetic and mechanical stress values of each sample point obtained by design of experiment are calculated by using the finite element method, and the sample points are fitted into different surrogate models, a set of surrogate models with minimum error is selected by using error evaluation indexes. Then, NSGA-II algorithm is used to optimize and select the optimal solution based on the fitted models. Compared with the initial design, the efficiency increased by 0.13%, the cost decreased by 3.84%, and the torque ripple decreased by 2.52%. Finally, the load experiment of the prototype is carried out, and the efficiency measured by the experiment is very close to the efficiency calculated. This paper can be used as a reference for the optimization design of HSIPMM.

REFERENCES

[1] D. Gerada, A. Mebarki, N. L. Brown, C. Gerada, A. Cavagnino and A. Boglietti, "High-Speed Electrical Machines: Technologies, Trends, and Developments," *IEEE Transactions on Industrial Electronics*, vol. 61, no. 6, pp. 2946-2959, Jun 2014.

[2] R. Tang, W. Tong, X. Han, "Overview on amorphous alloy electrical machines and their key technologies," *Chinese Journal of Electrical Engineering*, vol. 2, no. 1, pp. 1-12, 2016.

[3] J. Dong, Y. Huang, L. Jin and H. Lin, "Comparative Study of Surface-Mounted and Interior Permanent-Magnet Motors for High-Speed Applications," *IEEE Transactions on Applied Superconductivity*, vol. 26, no. 4, pp. 1-4, June 2016.

[4] X. WANG, L. ZHANG, W. XU, "Multi-objective Optimal Design for Interior Permanent Magnet Synchronous Motor Based on Taguchi Method," *Micromotors*, vol. 49, no. 5, pp. 1-5, 2016.

[5] W. Zhao, X. Wang, C. Gerada, H. Zhang, C. Liu and Y. Wang, "Multi-Physics and Multi-Objective Optimization of a High Speed PMSM for High Performance Applications," *IEEE Transactions on Magnetics*, vol. 54, no. 11, pp. 1-5, Nov. 2018.

[6] A. WANG, Y. WEN, "Optimal Design of Interior Permanent Magnet Synchronous Motor Based on Hybrid Genetic Algorithm," *Electric Machine and Control Application*, vol. 44, no. 3, pp. 59-65+95, Nov. 2018.

[7] J. CHEN, H. CHEN, Y. GAO, X. SUN, C. ZHANG and Z. JIANG, "Optimization Design of Amorphous Alloy Permanent Magnet Synchronous Motor for Electric Vehicle Based on Response Surface Method," *Micromotors*, vol. 54, no. 6, pp. 33-37, 2018.

[8] W. Wang, "Magneto-thermal coupling analysis and multi-objective structure optimization design of permanent magnet synchronous motor," M.S. thesis, Dept. Electron. Eng., Qingdao Univ., Qingdao, China, 2021.

[9] C. ZHANG, J. ZHU, W. TONG and X. Han, "Strength analysis and design of high speed interior permanent magnet rotor," *Electric Machines and Control*, vol. 21, no. 12, pp. 43-50, 2017.

[10] S. Li, Y. Li, W. Choi and B. Sarlioglu, "High-Speed Electric Machines:

Challenges and Design Considerations," *IEEE Transactions on Transportation Electrification*, vol. 2, no. 1, pp. 2-13, Mar 2016.

[11] L. SUN, X. ZHOU, "Loss Analysis of Permanent Magnet Synchronous Motor," *Electric Engineering*, vol. 2019, no. 20, pp. 159-161, 2019.

Shengnan Wu (M'18) was born in Yingkou, China. She received the B.S., M.S., and Ph.D. degrees in electrical engineering from the Shenyang University of Technology, Shenyang, China, in 2008, 2011, and 2017, respectively.

She is currently a Postdoctoral Research Assistant in electrical engineering with Shenyang University of Technology. Her research interests include electromagnetic design and multiphysical field simulation and analysis of permanent magnet machines.

Xiangde Sun was born in Liaoning, China. He received the B.S. degree in electrical engineering from Shenyang University of Technology, Shenyang, China, in 2020.He is currently working toward the M.S. degree in electrical engineering with the Shenyang University of Technology, Shenyang, China.

His main research interests include multi-physical field simulation and optimization of permanent magnet machines.

Wenming Tong (M'18) was born in Dandong, China. He received the B.S. and Ph.D. degrees in electrical engineering from the Shenyang University of Technology, Shenyang, China, in 2007 and 2012, respectively.He is currently an Associate Professor with the National Engineering Research Center for Rare Earth Permanent Magnet Machines, Shenyang University of Technology.

His major research interests include the design, analysis, and control of high-speed and low-speed direct drive permanent magnet machines, axial flux permanent magnet machines, hybrid excitation machines, and high-performance machines with new types of soft magnetic materials.